Methods 162–163 (2019) 23–30

Contents lists available at ScienceDirect

Methods

journal homepage: www.elsevier.com/locate/ymeth

Tracking of single tRNAs for translation kinetics measurements in chloramphenicol treated bacteria

Ivan L. Volkov[1], A. Carolin Seefeldt[1], Magnus Johansson*

Department of Cell and Molecular Biology, Uppsala University, Uppsala, Sweden

ARTICLE INFO

Keywords:
Protein synthesis
Translation
Single-molecule tracking
tRNA
In vivo
Chloramphenicol
Chloramphenicol resistance

ABSTRACT

Chloramphenicol is a broad-spectrum antibiotic targeting the protein synthesis machinery by binding to the bacterial ribosome. Chloramphenicol has been considered a classic general inhibitor of translation, blocking the accommodation of aa-tRNA into the A site of the large ribosomal subunit. However, recent studies suggest that this proposed mechanism is a simplification and that the effect of chloramphenicol on mRNA translation is much more dynamic. By tracking single dye-labelled elongator and initiator tRNAs in *Escherichia coli* cells treated with chloramphenicol, we observe the direct effect of chloramphenicol on translation kinetics. We find clear indications of slow but significant mRNA translation on drug bound ribosomes.

1. Introduction

Ribosome catalyzed protein synthesis lies at the very heart of life as we know it. Decades of biochemical and structural approaches using reconstituted systems have led to a detailed picture of how ribosomes translate the genetic information on mRNAs into proteins (see e.g. Ref. [1] for a recent review). Due to its central role, the bacterial protein synthesis machinery is also one of the most common targets for antibiotic drugs [2]. Reconstituted systems have here helped in mapping the binding sites of a large array of antibiotic drugs, and their inhibitory actions have been investigated using a wide variety of in vivo and in vitro methods. However, despite these efforts, there are still clear gaps in our understanding of how several of these antibiotics actually prevent bacterial cell growth or proliferation. For example, over the last 30 years the traditional model of ribosome inhibition by macrolide drugs, such as erythromycin, has been challenged and is now currently being revised. Rather than simply operating as a plug in the nascent peptide exit tunnel [3], the tunnel-bound macrolide discriminates nascent peptides in a sequence specific manner [4–7]. Hence, even in the presence of saturating macrolide concentrations, there is significant ongoing protein synthesis in the cell [5–7], which implies that the inhibitory action might be due to a disruptive radical change in the proteome rather than a complete protein synthesis shut-down [5–7].

Similar to the recent revision of our understanding of macrolide action, the mechanism of action of the antibiotic drug chloramphenicol (CHL) is currently being scrutinized. CHL was one of the earliest broad-spectrum antibiotics, introduced in the late 1940s [8], and has since been used to treat e.g. bacterial meningitis [9]. Nowadays, CHL is mainly used to treat eye infections and is recommended by the WHO as a second line antibiotic due to its severe side effects (reviewed in reference [9]). The drug is also regularly used in molecular biology laboratories for selection of e.g. successful plasmid transformation [10]. CHL has commonly been considered a classic translation elongation inhibitor, blocking the peptidyl transfer reaction (e.g. [11,12]). Addition of the drug to growing bacterial cell cultures resulted in stable polysomes [13], and the CHL binding site on the 50S, as shown by X-ray crystallography [11,12], suggested a clear competitive inhibition of aa-tRNA binding in the PTC of the 50S subunit A site. In early ribosome profiling experiments in bacteria, CHL was also used as a “general” translation elongation inhibitor to produce a snapshot of ribosome footprints on the complete transcriptome [14]. However, accumulated evidence suggest that this static view of CHL action is a simplification. Very early in vitro biochemical experiments indicated that incorporation of aromatic amino acids into the polypeptide chain were less severely inhibited by CHL than other amino acids [15]. Further, the expression of some CHL resistance genes requires CHL mediated stalling of ribosomes on short 5’ leader ORFs, suggesting the synthesis of short peptides by CHL bound ribosomes [16,17]. More

Abbreviations: CHL, Chloramphenicol; CAT, Chloramphenicol acetyl transferase; HMM, Hidden Markov Model; PTC, Peptidyl transferase centre; WHO, World Health Organization; CFU, Colony Forming Unit; AIC, Akaike information criterion; RDM, EZ Rich Defined Medium

* Corresponding author.
E-mail address: m.johansson@icm.uu.se (M. Johansson).
[1] These authors contributed equally.

https://doi.org/10.1016/j.ymeth.2019.02.004
Received 7 December 2018; Received in revised form 1 February 2019; Accepted 5 February 2019
Available online 08 February 2019

recently, a thorough systematic study of CHL effects using ribosome profiling together with in vitro toe printing showed that the elongation inhibition of CHL is highly dependent on both the nascent peptide sequence as well as the A-site acceptor amino acid [18]. In conjunction with a recent molecular dynamics study, suggesting the binding site of CHL on tRNA bound ribosomes to be different from the site suggested from X-ray crystallography of CHL bound ribosomes lacking tRNAs [19], these results certainly point towards an inhibitory action by CHL resembling more that of the macrolides, namely sequence specific inhibition of translation elongation. Hence, these recent findings definitely call for additional studies of CHL action with a new set of glasses.

The static view of antibiotics as general inhibitors of a specific step in protein synthesis might reflect more the detection methods rather than the drug action itself. Although structural insights in combination with kinetics studies using reconstituted systems can definitely aid in providing a functional quantitative understanding [2,20], these studies are still most often confined to a very particular context (e.g. the synthesis of specific di- or tri-peptides). In addition, with reconstituted systems there is always a potential risk of missing out some key component present inside the cell, in particular when the mechanism of interest is as complex as the translation apparatus. Studies of reaction kinetics inside living cells, on the other hand, have been challenging because the molecules of interest are normally not synchronized but work under steady-state conditions. Artificial synchronization methods have been developed, e.g. using the β-galactosidase induction assay [21,22] to measure average translation rates on specific mRNAs. Such experiments, however, only provide indirect information on full-length protein synthesis, and also in a very specific context. With recent years' development of in vivo single-molecule methods however, the need for synchronization disappears, and we are finally getting equipped with methods to observe dynamic inter-molecular processes directly inside living cells (see e.g. [23] for a recent review related to protein synthesis dynamics).

We have recently demonstrated how tRNA molecules, in vitro labelled with small organic dyes, can be electroporated back into living *E. coli*cells and studied using super-resolved single-molecule tracking [24]. By combining the superior photophysical properties of small organic dyes, with new Hidden Markov Model (HMM) based analysis methods to detect fluorophore transitions between different diffusional states, we were able to measure the time the tRNAs spent bound on ribosomes, and hence achieving a direct measurement of translation kinetics on single ribosomes inside living cells. In the present study, we apply this method to investigate the effect of CHL on translation initiation and elongation kinetics. In agreement with recent studies, we find that presence of CHL does allow dynamic exchange of both [Cy5]tRNA^{fMet} and [Cy5]tRNA^{Phe} on ribosomes, suggesting ongoing translation, albeit at slower pace.

2. Materials and methods

2.1. Preparation of labelled and aminoacylated tRNA

tRNA^{Phe} and tRNA^{fMet} from *E. coli* were labeled site specifically [25] with disulfo-Cy5 mono-reactive NHS or maleimide dyes (hereafter referred to as Cy5) on the naturally occurring 3-(3-amino-3-carboxypropyl)uridine in position 47, and 4-thiouridine in position 8, respectively. Labeled tRNAs were aminoacylated (and formylated for tRNA^{fMet}), and purified by HPLC as described previously [24]. For labeling of tRNA^{fMet}, we noticed that, in our hands, even a small amount of DMSO (~2%) in the labeling mixture alters the mobility of the tRNA on RP-HPLC and hampers subsequent aminoacylation of [Cy5]tRNA^{fMet}. We speculate that this is caused by DMSO induced tRNA misfolding. For this reason, it is recommended to use dry aliquots of the dye for labeling reactions. In case of tRNA^{Phe}, 2% of DMSO in the labeling mixture did not affect the tRNA functionality. Final yields after labeling, aminoacylation and HPLC purification were about 6% for tRNA^{Phe} and 1% for tRNA^{fMet}. Aminoacylated and labeled tRNA samples were stored in frozen aliquots (2 pmol) at −80 °C.

2.2. Growth media

EZ Rich Defined Medium (RDM, from Teknova) with 0.2% (w/v) glucose as carbon source, was reconstituted, aliquoted (5 ml) and stored frozen at −20 °C. For each experiment, freshly thawed and filtered (0.2 μm) RDM was used. SOB medium, lacking Mg^{2+} (2.0% (w/v) tryptone, 0.5% (w/v) yeast extract, 10 mM NaCl, 2.5 mM KCl, pH 7.0), M9 (37.5 mM Na_2HPO_4, 2.2 mM KH_2PO_4, 8.5 mM NaCl, 18.65 mM NH_4Cl, 2 mM $MgSO_4$, 0.1 mM $CaCl_2$, 0.4% (w/v) glucose, 1x RPMI 1640 amino acids, 10 μM thiamine) and LB-Miller (1% (w/v) tryptone, 0.5% (w/v) yeast extract, 170 mM NaCl) were prepared in house.

2.3. Preparation of electrocompetent cells, electroporation and microscopy

ElectroMAX DH5α-E *E. coli* cells (supplied electrocompetent by Invitrogen), referred to as DH5α in the main text, were thawed on ice, diluted 5 times with 10% (v/v) glycerol water solution (final $OD_{600} \approx 60$), aliquoted (20 μl) and frozen in dry ice-EtOH bath for long term storage at −80 °C. Electroporation of these cells was carried out without further manipulations.

Modified DH5α cells supplemented with the pBAD33 plasmid, carrying the CHL acetyl transferase gene, *cat* (one of the most common resistance genes against CHL and used as a selectivity marker in plasmids [10]), were made electrocompetent in house based on the method suggested in reference [26]. Cells were grown in 50 ml SOB medium (lacking Mg^{2+}) at 37 °C, until they reached OD_{600} = 0.2–0.4, then chilled in ice-water bath for 20–40 min. All later steps were performed in the cold room (4 °C). Cells were pelleted by centrifugation in 50 ml falcon tubes (2000 × *g*, 10 min). The supernatant was removed and cells were resuspended in the same falcon tubes (50 ml) in 10% (v/v) glycerol water solution using cut pipette tips (providing bigger holes and thus less disturbance for cells) and pelleted (1500 × *g*, 10 min). The pelleted cells were then washed an additional three times by dissolving and centrifugation (1000 × *g*, 5 min) in 2 ml tubes. It is utterly important to remove as much of the supernatant as possible (sacrificing cells) in order to achieve lower final salt concentration. After the final wash, the cells were resuspended in 120–150 μl of 10% (v/v) glycerol and a test electroporation of a pure cell sample was performed (as described below). If the resulted electroporation time constant is low (in our case we chose a cutoff of 5.8 ms), washing should be repeated to achieve higher resistivity of the cell sample. After washing, the cell density was adjusted to OD_{600} 60 ± 10, cells were aliquoted (20 μl), and finally frozen in EtOH/dry ice bath for storage. By performing electroporation efficiency tests using a pUC19 plasmid (Invitrogen) followed by selection on ampicillin plates, we noticed that the CFU (colony-forming unit) depended on freezing method according to: no freezing > snap freezing in EtOH-dry ice bath > slow freezing in −80 °C freezer > snap freezing in liquid N_2. By performing similar tests on electrocompetent cells prepared in different media, i.e. LB, M9, RDM (0.2% glucose), and SOB (lacking Mg^{2+}), we found SOB to be the best, in agreement with previous conclusions suggesting that the medium should be rich in nutrients and low in ionic strength [26].

For electroporation, 20 μl of cells (OD_{600} = 60 ± 10) were mixed with 2 pmol dye-labeled tRNA and incubated on ice for 1 min. The sample was transferred into an ice-cold 1 mm electroporation cuvette (Molecular Bio Products or VWR). Electroporation was performed using a MicroPulser instrument (Bio-Rad) by applying a 1.9 kV pulse which typically resulted in a decay time constant of 5.8 ± 0.2 ms. 500 μl of RDM (room temperature) was immediately added to the cuvette. Lower time constant or arcing are usually results of excess salts in the sample, which cause cell death and lower electroporation efficiency. Thus, attention should be paid to amount of salts in the final electroporation

mixture. Cells were allowed to recover for 30 min on heating block at 37 °C. The cells were then harvested by centrifugation (1200 × *g*, 2 min) and washed 3 times with 37 °C RDM medium to remove non-internalized tRNA. Cells were re-suspended in RDM to OD_{600} = 0.03, spread onto a 2% agarose pad (0.6 μl cell suspension to a ~ 25 mm^2 pad) containing RDM and 1 μM of SYTOX Blue dead-cell stain (Invitrogen), and placed under the microscope (approximately 60 min after electroporation). The temperature of the sample was maintained at 37 ± 2 °C using a cage incubator encapsulating the microscope stage. The sparsely spread out single cells on the pad were allowed to grow and divide to form mini-colonies, and RDM supplemented with 5 μg/ml or 100 μg/ml CHL and 1 μM SYTOX blue was injected to the sample 100 min after the microscopy sample had been prepared. Fluorescence imaging was performed 70–200 min after CHL injection. The incubation time was chosen based on our previous results from tRNA tracking in rifampicin treated cells [24], where 70 min was enough to completely abolish translation. In a control experiment with a dye of approximately the same molecular weight as CHL, acridine orange, > 80% of the maximal signal was reached in the middle of the agarose pad after 70 min (Fig. S1).

For fluorescence imaging of the cell strain containing the pBAD33 plasmid, the agarose pad did already from the beginning contain 5 μg/ml CHL. Imaging was here performed when single cells had grown and divided to form colonies of 4–8 cells, i.e. 90–180 min after microscopy sample preparation.

Each microscopy experiment contains pooled data from 2 to 5 replicas (each comprising 20–120 cell colonies with internalized [Cy5] tRNA, see Supplementary Table 1 for number of replicas) performed on different dates, using the same batches of electrocompetent cells and labeled tRNAs.

The raw data for [Cy5]$tRNA^{Phe}$ and [Cy5]$tRNA^{fMet}$ diffusion in non CHL treated DH5α were obtained earlier [24] using the same experimental routine.

2.4. Optical setup

An inverted Nikon Ti-E microscope equipped with a Nikon CFI Apo TIRF 100x 1.49NA objective and an additional 2.0x lens (Diagnostic Instruments DD20NLT) in front of the camera was used. Bright-field and fluorescence images were acquired using an Andor iXon 897 Ultra EMCCD camera. For phase contrast acquisition, a Lumenera Infinity 2–5 M camera was used. [Cy5]tRNA tracking was performed using a 639 nm laser (Coherent Genesis MX 639-1000 STM) with an output power density of 5 kW/cm^2 on the sample plane in stroboscopic illumination mode with 1.5 ms laser/5 ms camera exposures. A 405 nm laser (Cobolt MLD) with an output power density of 4 W/cm^2 on the sample plane with continuous exposure of 21 ms was used for SYTOX Blue imaging. The microscope was operated using μManager 1.4.20 software, and automated acquisitions were made using a μManager plugin made in-house.

2.5. Single particle tracking

The procedure for data analysis has been described in detail previously [24]. In brief, cells were segmented by extracting cell outlines from phase contrast images using the algorithm published in reference [27], and incorrectly segmented or dead (SYTOX stained) cells were manually removed. For practical reasons, fluorescence movies of colonies with no or very few fluorescent tRNAs (≤2 fluorophores per cell colony) were not included in the analysis. On a few occasions (≤5 cells per dataset), cells with spots completely immobilized for longer than 100 frames with intensities much lower than single Cy5 fluorophore (fluorescent impurities) or much higher (not a single fluorophore), were omitted from the analysis.

Fluorescent spots were detected using the radial symmetry-based method [28], as implemented in [29]. Spot positions were thereafter refined and position uncertainties were estimated using a symmetric Gaussian spot model and the maximum aposteriori fit [30]. Trajectories were built using uTrack [31] allowing gaps of 3 missing points. For trajectory building, we excluded spots > 3 pixels outside live cells, spots with width (std) > 280 nm, spots with amplitute < 50 photons, and spots in cells with > 2 spots in current and future frames.

To extract diffusion properties from the trajectories we used an HMM algorithm [30] which fits ensembles of trajectories for each experimental condition to a global model of fixed size. The algorithm handles missing positions and makes explicit use of positions as well as localization uncertainties of each position [30]. The procedure is the same as described in more detail previously [24], except that the subsequent pruning of states, to find smaller models, was not included. To select the optimal model size, i.e. number of diffusive states, we used the Akaike information criterion [32]. To condense an HMM with many states to an effective two-state description, the hidden states were classified as “fast” (freely diffusing tRNA or tRNA in complex with EF-Tu) or “slow” (ribosome-bound) using a threshold value of 1 $\mu m^2/s$.

2.6. Cell growth rates in bulk

E. coli DH5α cells were grown overnight in RDM at 37 °C. The overnight culture of *E. coli* DH5α cells with the pBAD33 plasmid was supplemented with 34 μg/ml of CHL. 0.2 μl of overnight cultures were then inoculated in 200 μl of fresh preheated RDM containing different concentrations of CHL on a 96-well microplate and were grown at 37 °C in a microplate reader (Infinite M200, Tecan). Optical densities at 600 nm were measured with a prior 1 min orbital shaking every 5 min during 24 h. Wells filled with 200 μl RDM media were used as blank.

2.7. Cell growth rates on the microscope

Samples for the microscopy (including antibiotic injection, if applicable) were prepared as described above, but electroporations were made without tRNA added. Individual cell colonies were imaged in phase contrast regime every 10 min, cell contours were detected as described above and cell areas (2D projection) were calculated. Growth curves within the time interval corresponding to tracking data acquisition were fitted by a single exponential function using MagicPlot (MagicPlot Systems). Positions containing cells with no obvious growth and time points with cell segmentation artifacts were omitted from the analysis.

3. Results and discussion

3.1. Effect of CHL on [Cy5]$tRNA^{Phe}$ binding kinetics

To investigate the effect of CHL on translation elongation kinetics, we employed our recently developed strategy to measure dwell times of dye labelled tRNAs on ribosomes inside living cells. As shown previously, [Cy5]$tRNA^{Phe}$ in *E. coli* cells growing on rich medium agarose pads display a diffusion pattern consistent with repeated utilization on elongating ribosomes (Fig. 1). The measured dwell time of [Cy5]$tRNA^{Phe}$ in the ribosome bound state, 100 ms on average [24], was in perfect agreement with previous in vivo and in vitro estimates of the average elongation rate [33,34], provided that deacylated tRNA

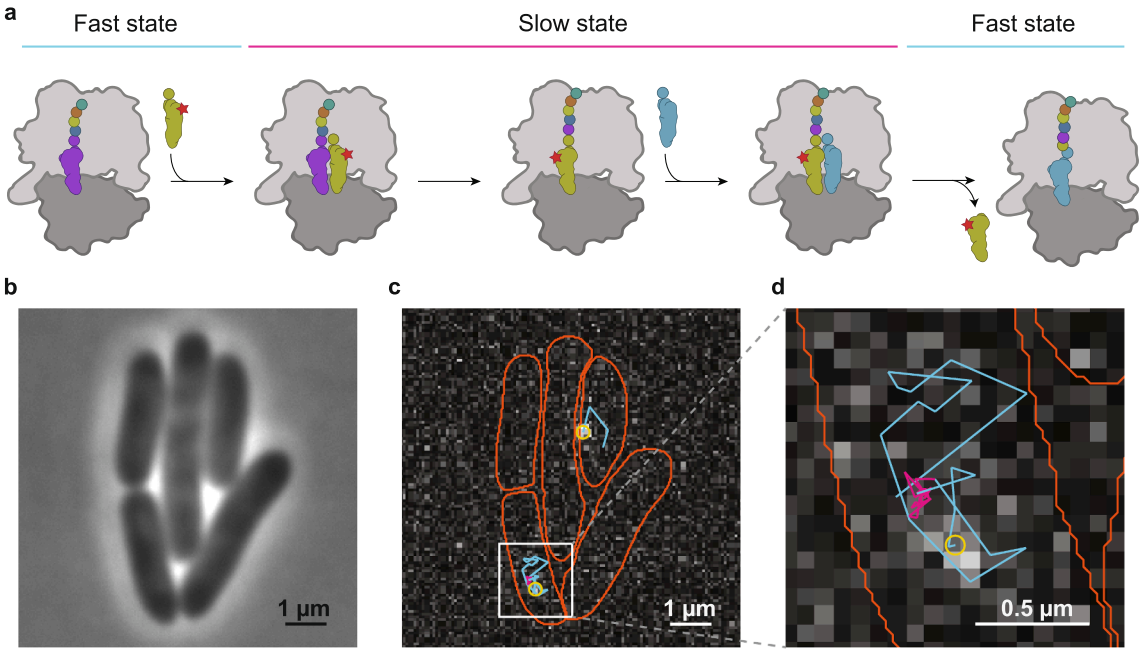

Fig. 1. Single tRNA tracking for translation kinetics measurements in live *E. coli* cells. (a) Expected diffusion of [Cy5]tRNA^{Phe}(red star) being used on a translating ribosome: fast state for free tRNA or tRNA in complex with GTP and EF-Tu, and slow state for tRNA bound to a ribosome during two elongation cycles. The detected dwell time on ribosomes is used as a measure of the translation elongation time. (b) Phase contrast image of a small colony of DH5α cells, grown from a single electroporated cell. (c) A selected frame from a fluorescence movie with cell contours (orange), current fluorophore position (yellow circles), and detected [Cy5]tRNA^{Phe} trajectories. Trajectories are color-coded with respect to diffusion state (fast = cyan, slow = magenta), estimated from HMM based analysis. (d) Magnification of region from panel c showing an apparent binding event of approximately 100 ms. (For interpretation of the references to color in this figure legend, the reader is referred to the web version of this article.)

dissociates rapidly from the ribosome E site [35]. Further, experiments in a ribosome mutant strain, known to display slow translation elongation, resulted in twofold longer dwells of [Cy5]tRNA^{Phe} in the slowly diffusive state [24], suggesting that this dwell time serves as a good proxy for the translation time of individual ribosomes.

According to the traditional model of CHL action, CHL is inhibiting aa-tRNA accommodation into the PTC of the 50S A site non-discriminatory and completely. In cells subjected to CHL we would therefore expect to have one fraction of tRNA^{Phe} bound stably to the P site of ribosomes, and the remainder freely diffusing as naked tRNA or bound in ternary complex with GTP and EF-Tu. We might as well expect short lived binding attempts of tRNA^{Phe} to ribosome A sites (< 10 ms if aa-tRNA dissociates directly after GTP-hydrolysis [36]), below our detection range. Based on reported tRNA/ribosome stoichiometry [37] and Phe codon usage [37], we would then estimate 15–25% of the total tRNA^{Phe} pool to be bound to ribosome P sites at any given moment in growing *E. coli* cells. To test this model, we electroporated [Cy5]tRNA^{Phe} into DH5α *E. coli* cells and placed the cells on RDM agarose pads under the microscope for incubation at 37 °C. After individual cells had grown to small colonies, we injected solutions containing 5 μg/ml or 100 μg/ml CHL to the cell samples. In bulk liquid culture, the lower CHL concentration results in slow but detectable growth of DH5α cells (Fig. S2), whereas at the higher concentration, cell growth is practically completely inhibited (Fig. S2). Reported MIC values for susceptible *E. coli* are in the 1–8 μg/ml range [38–40]. On agarose pads, we noted that cells treated with 5 μg/ml CHL continued growing, although at much slower rate (volume doubling time ~150 min, compared to ~50 min on pads in absence of CHL), and with altered cell division, often resulting in longer cells. The cells treated with 100 μg/ml CHL concentration did not display growth at all, and a small fraction, 1–2%, lyzed during incubation in presence of CHL. The cells on the agarose pads were incubated for 70 min in presence of CHL, and fluorescence movies were subsequently acquired.

Applying our single-molecule tracking pipeline on acquired microscopy movies, we are able to follow individual [Cy5]tRNA^{Phe} molecules through transitions between different diffusive states, where the Hidden-Markov Model based analysis of the resulting trajectories provides us with average occupancies and dwell times of the dye-labelled molecules in the separate states. The best model size, i.e. number of diffusive states, according to AIC (6–8 states), is for simplicity coarse-grained to a 2-state model representing ribosome bound or free tRNA (see Section 2.5, and reference [24]). The threshold for this coarse-graining, 1 μm^2/s, was chosen based on previous analyses of ribosome diffusion [41–43] as well as our own earlier tRNA tracking results [24]. The best multistate models for all experimental datasets are shown in Supplementary Table 1 along with their corresponding coarse-grained 2-state models.

Compared to tracking results in untreated cells, the diffusive behaviour of [Cy5]tRNA^{Phe} in cells treated with CHL is clearly distinct. In cells subjected to 5 μg/ml CHL, the occupancy of [Cy5]tRNA^{Phe} in the ribosome bound state decreased from 17% to 8% compared to in untreated cells (Fig. 2b), whereas the average dwell time in the bound state increased roughly twofold, to 220 ms (+/− 30 ms, Fig. 2c). At 20 times higher CHL concentration, 100 μg/ml, the occupancy in the bound state is further decreased to 6% (Fig. 2b), and the average dwell time increased to 290 ms (+/− 60 ms, not significantly higher than at 5 μg/ml CHL, Fig. 2c). Whereas the bound-state dwell time at the lower CHL concentration might represent an average over two populations, i.e. one CHL bound fraction of ribosomes with immobilized [Cy5]tRNA^{Phe}, and a second fraction of ribosomes elongating at normal speed, we would then at 100 μg/ml of CHL expect to have a practically uniform CHL bound population of ribosomes. This hypothesis is in line with the reported dissociation constant for CHL binding to ribosomes, K_d = 2 μM (i.e. 0.6 μg/ml) [44], if we assume that the reported 10 fold decrease in MIC upon TolC efflux pump deletion [38] implies that functional TolC (present in DH5α) lower the intracellular concentration

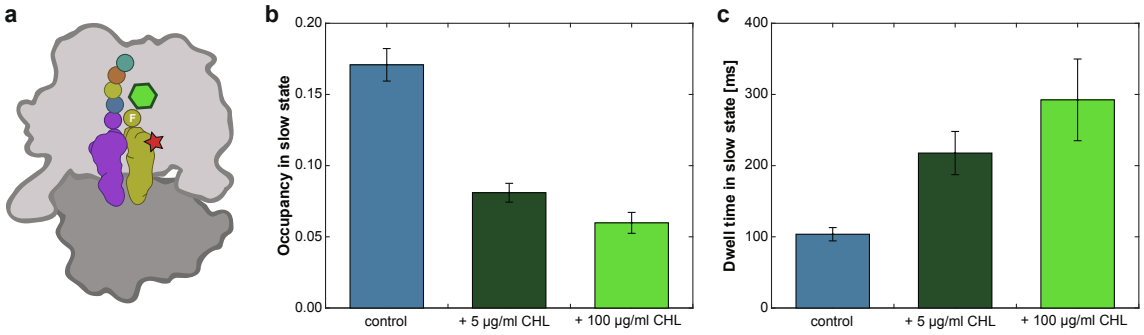

Fig. 2. Effect of CHL on [Cy5]tRNA^{Phe} binding to ribosomes (a). (b) HMM estimated occupancy and (c) dwell time of [Cy5]tRNA^{Phe} in the ribosome bound state. Experiments were performed in the absence of CHL (n = 17,286, raw data from [24]), or presence of 5 µg/ml (n = 30,153) or 100 µg/ml (n = 32,832) CHL, respectively. Error bars represent bootstrap estimates of standard errors.

of CHL a factor of 10 in this concentration range (i.e. from 5 µg/ml and 100 µg/ml to 0.5 µg/ml and 10 µg/ml, respectively). Further, the fact that a 20-fold increase in CHL concentration did not affect the slow state occupancy and dwell time significantly, strongly suggest that CHL binding to ribosomes is saturated at the higher concentration.

The finite dwell time in the slow state at 100 µg/ml CHL, confirmed by observations of transitions of [Cy5]tRNA^{Phe} to and from the ribosome bound state (Supplementary Movie 1 and deposited data), thus clearly shows a dynamic exchange of [Cy5]tRNA^{Phe} on ribosomes, which might suggest that protein synthesis is occurring even in the presence of CHL at growth inhibiting concentrations. Elongation on individual ribosomes, however, seems to be slowed down approximately threefold, at least on Phe codons. We can further use the slow-state occupancy and dwell time, to calculate the usage frequency of tRNA^{Phe} on ribosomes, from which we then estimate that the overall protein synthesis rate inside the cells have decreased to 22% and 13% of that in untreated cells for 5 µg/ml CHL and 100 µg/ml CHL, respectively.

It should also be noted that in our previous tracking experiments with [Cy5]tRNA^{Phe} in cells treated with rifampicin (which inhibits transcription) the occupancy in the ribosome bound state was less than 1%, indicating that [Cy5]tRNA^{Phe} does not bind unspecifically to non-elongating ribosomes [24].

Hence, from our [Cy5]tRNA^{Phe} tracking experiments we conclude that even at growth inhibiting concentrations of CHL we do observe a dynamic exchange of [Cy5]tRNA^{Phe} on ribosomes, suggesting slow but ongoing mRNA translation, in line with recent results [18]. However, an alternative explanation to our observation at this point could be that the detected association-dissociation events represent long-lived unproductive bindings to the A site of stalled ribosomes, terminated by a mechanism similar to proofreading.

3.2. Effect of CHL on [Cy5]tRNA^{fMet} binding kinetics

To further investigate the effect of CHL on protein synthesis kinetics, we used CHL to treat cells electroporated with Cy5 labelled initiator tRNA^{fMet}. From the traditional static model of CHL action we would again expect to see a snapshot of P-site bound tRNAs, locked by drug inhibition of aa-tRNA binding to the A site. With less start codons than Phe codons in the transcriptome [37], and more competing dark tRNAs [37], the fraction of tRNA^{fMet} bound to ribosomes at any given moment in growing cells is significantly lower than that of tRNA^{Phe} [24]. On the other hand, one might also suspect that the additional "idle" pool of ribosomes (~15% [45]), normally not mRNA bound at a particular moment, would be able to initiate and bind tRNA^{fMet} in the P sites even in the presence of completely inhibiting concentrations of CHL, but stall as stable 70S initiation complexes. Considering this, the number of tRNA^{fMet} inside the cell is only approximately twice as many as potentially initiating ribosomes [37]. In the presence of CHL, and if there are enough mRNAs for these idle ribosomes, we would then actually expect half of all [Cy5]tRNA^{fMet} stably bound to ribosomes.

From the HMM analysis of [Cy5]tRNA^{fMet} trajectories in cells subjected to CHL we find that the binding pattern of the initiator tRNA also gets affected by the drug. The dwell time of [Cy5]tRNA^{fMet} on ribosomes, which includes the time for 50S subunit joining (estimated previously as 20 ms [24]) and the time for the first elongation cycle, increases almost twofold in the presence of 5 µg/ml and 100 µg/ml CHL compared to in non-treated cells (Fig. 3c), i.e. 120–130 ms versus 70 ms. This increase in dwell time could be due to some unknown effect of CHL on translation initiation, but is more likely a result of the general slowdown in elongation observed with [Cy5]tRNA^{Phe}. If so, this means that CHL affects already the formation of the first peptide bond, contrary to previous observations based on the toe-print assay [18].

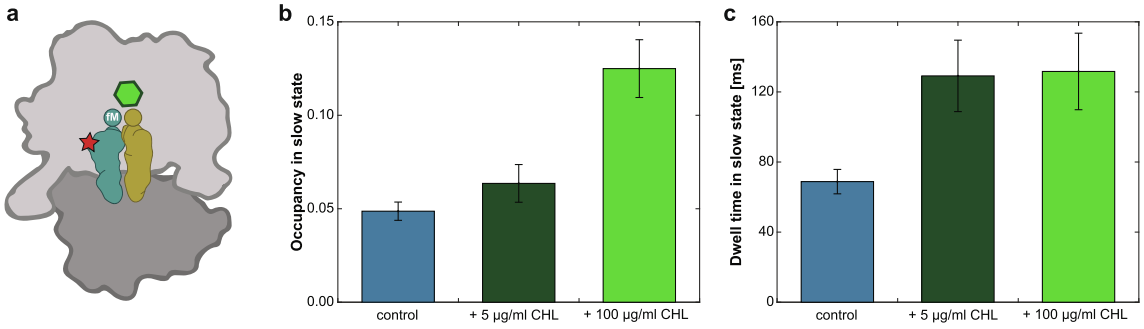

Fig. 3. Effect of CHL on [Cy5]tRNA^{fMet} binding to ribosomes (a). (b) HMM estimated occupancy and (c) dwell time of [Cy5]tRNA^{fMet} in the ribosome bound state. Experiments were performed in the absence of CHL (n = 31,498, raw data from [24]), or presence of 5 µg/ml (n = 21,192) or 100 µg/ml (n = 15,680) CHL, respectively. Error bars represent bootstrap estimates of standard errors.

However, with only a twofold decrease of the rate on average (i.e. 100–110 ms for the first elongation cycle instead of 50 ms [24]), this effect would most probably be hidden in those experiments [18].

The fact that we do observe a dynamic exchange also of [Cy5]tRNA^{fMet} on ribosomes, provides additional indications of ongoing mRNA translation in CHL treated cells. As already discussed, complete inhibition of A-site binding of elongator tRNAs would most probably result in a high fraction of tRNA^{fMet} stably bound to initiating ribosomes. From experiments in reconstituted systems we further know that the 70S initiation complex and even the 30S pre-initiation complex (i.e. mRNA bound 30S with fMet-tRNA^{fMet} in P site) are very stable in different buffer systems [4,46]. Hence, we would not expect repeated binding and dissociation events of tRNA^{fMet} without productive elongation. With this reasoning we also conclude that the dynamic ribosome binding events observed with elongator [Cy5]tRNA^{Phe} most likely, at least to some extent, represent productive events as well, rather than non-productive proofreading events. Extensive proofreading of cognate tRNAs could however explain longer than normal dwell times during productive tRNA binding. That is, once the labelled tRNA^{fMet} or tRNA^{Phe} is bound to the ribosomal P site, extensive proofreading of incoming aminoacyl-tRNAs into the A site would slow down the process.

Further, from the HMM analysis of the [Cy5]tRNA^{fMet} trajectories we find that the occupancy in the slow, ribosome bound state increase with increasing CHL concentration (Fig. 3b). Since the average dwell time of [Cy5]tRNA^{fMet} on ribosomes is approximately the same at both CHL concentrations, this result suggests more initiation events per cell per time unit with higher CHL concentration. For [Cy5]tRNA^{Phe}, we see the opposite effect, i.e. fewer binding events with increasing CHL concentration (higher dwell time but lower occupancy). Taken together these results thus suggest more initiation events per elongation event, which, we speculate, might be due to premature termination of translation in presence of CHL.

3.3. Effect of CAT on CHL action

Finally, to investigate the effect of the widely used chloramphenicol resistance gene *cat* (encoding a chloramphenicol acetyl transferase) on translation, we tracked [Cy5]tRNA^{Phe} in cells harbouring the pBAD33 plasmid (containing *cat*) equilibrated with 5 μg/ml CHL. Based on the dwell time and occupancy of [Cy5]tRNA^{Phe} on ribosomes in these experiments (Fig. 4) we conclude that CAT efficiently deactivates CHL, and that protein synthesis is recovered to normal levels in the resistant cells—with respect to the average elongation rate per ribosome as well as the overall frequency of Phe codon readings per cell.

4. Conclusions

In the present study we have used our new tools for live cell kinetics measurements of ongoing protein synthesis to investigate the inhibitory effect of the widely used antibiotic drug CHL on translating ribosomes. At high CHL concentration, where we expect to have all ribosomes bound by CHL, we still find a dynamic exchange of both [Cy5]tRNA^{Phe} and [Cy5]tRNA^{fMet} on ribosomes, strongly suggesting that these ribosomes are still synthesizing peptides. Our results are in perfect agreement with recent reports suggesting incomplete and sequence specific inhibition of translation by CHL [18]. Although, with our current experimental method, we cannot confirm sequence-specific translation inhibition by CHL, our results provide additional evidence of ongoing mRNA translation on CHL bound ribosomes. We further propose that the average rate of elongation per ribosome decreases threefold in the presence of CHL (at least on Phe codons) and we present results compatible with a model in which CHL causes premature termination of translation. A potential explanation to both these observations could be that CHL to some extent, but not completely, inhibits accommodation of aa-tRNA to PTC, or the peptidyl transfer reaction itself, resulting in extensive proofreading of cognate tRNA. This would decrease the probability of productive tRNA binding to the ribosome (observed as a decreased occupancy of the ribosome bound state for [Cy5]tRNA^{Phe}) and thereby extending the dwell time of tRNA bound in the P site (fMet-[Cy5]tRNA^{fMet} or peptidyl-[Cy5]tRNA^{Phe}). Further, long tRNA dwell times in the ribosome P site might result in increased level of peptidyl-tRNA drop-off, in particular during the first elongation cycles [47,48], which would, upon recycling of the ribosome, result in a proportionally higher frequency of initiation per elongation cycle, in line with our findings. In the presence of CHL and the CHL resistance gene *cat*, the elongation rate and the overall protein synthesis rate are completely recovered to the levels in absence of CHL.

This study highlights the strength of single-molecule based studies of dynamic intra-molecular interactions inside living cells, where the high number of molecules working under steady-state complicates kinetics measurements in bulk. Our results also underscore the importance of kinetics studies of antibiotic actions. Limitations in experimental methods probing the dynamics of the protein synthesis system have perhaps led to somewhat naïve and simplistic models of CHL action in the past. We are optimistic that new single-molecule tracking based approaches will in the near future help to reveal many new insights into the inhibitory mechanisms of translation targeting antibiotics, as well as insights into resistance mechanisms against these compounds.

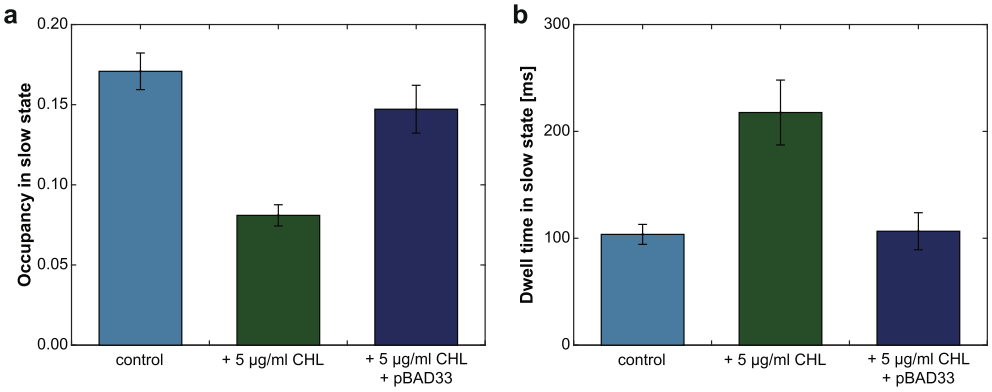

Fig. 4. Presence of the CHL resistance gene *cat* abolishes the effect of CHL. (a) HMM estimated occupancy and (b) dwell time of [Cy5]tRNA^{Phe} in the ribosome bound state in cells carrying the *cat* containing pBAD33 plasmid, grown on 5 μg/ml CHL pads (n = 8,279). Results from experiments in absence of the resistance gene (from Fig. 2) are shown for comparisons. Error bars represent bootstrap estimates of standard errors.

Acknowledgements

We thank the Dan Anderson group for providing the pBAD33 plasmid and Irmeli Barkefors for comments on the manuscript. This work was supported by The Swedish Research Council (M.J. 2015-04111, 2016-06264), and Carl Tryggers Stiftelse för Vetenskaplig Forskning (M.J. 15:243; M.J., A.C.S. 17:226).

Appendix A. Supplementary material

Supplementary data to this article can be found online at https://doi.org/10.1016/j.ymeth.2019.02.004. The raw data supporting this manuscript is available at the open research repository Zenodo: https://doi.org/10.5281/zenodo.2554853. Previously published raw data (Volkov et al. 2018, NatChemBiol), referred to in the present study, is available at: https://doi.org/10.5281/zenodo.1168228.

References

[1] M.V. Rodnina, The ribosome in action: Tuning of translational efficiency and protein folding, Protein Sci. 25 (2016) 1390–1406, https://doi.org/10.1002/pro.2950.
[2] D.N. Wilson, Ribosome-targeting antibiotics and mechanisms of bacterial resistance, Nat. Rev. Microbiol. 12 (2014) 35–48, https://doi.org/10.1038/nrmicro3155.
[3] J.R. Menninger, D.P. Otto, Erythromycin, carbomycin, and spiramycin inhibit protein synthesis by stimulating the dissociation of peptidyl-tRNA from ribosomes, Antimicrob. Agents Chemother. 21 (1982) 811–818 (Accessed November 20, 2018), http://www.ncbi.nlm.nih.gov/pubmed/6179465.
[4] M. Johansson, J. Chen, A. Tsai, G. Kornberg, J.D. Puglisi, Sequence-dependent elongation dynamics on macrolide-bound ribosomes, Cell Rep. 7 (2014) 1534–1546, https://doi.org/10.1016/j.celrep.2014.04.034.
[5] K. Kannan, N. Vázquez-Laslop, A.S. Mankin, Selective protein synthesis by ribosomes with a drug-obstructed exit tunnel, Cell 151 (2012) 508–520, https://doi.org/10.1016/j.cell.2012.09.018.
[6] K. Kannan, P. Kanabar, D. Schryer, T. Florin, E. Oh, N. Bahroos, T. Tenson, J.S. Weissman, A.S. Mankin, The general mode of translation inhibition by macrolide antibiotics, Proc. Natl. Acad. Sci. U. S. A. 111 (2014) 15958–15963, https://doi.org/10.1073/pnas.1417334111.
[7] A.R. Davis, D.W. Gohara, M.-N.F. Yap, Sequence selectivity of macrolide-induced translational attenuation, Proc. Natl. Acad. Sci. U. S. A. 111 (2014) 15379–15384, https://doi.org/10.1073/pnas.1410356111.
[8] K. Lewis, Platforms for antibiotic discovery, Nat. Rev. Drug Discov. (2013), https://doi.org/10.1038/nrd3975.
[9] G. Dinos, C. Athanassopoulos, D. Missiri, P. Giannopoulou, I. Vlachogiannis, G. Papadopoulos, D. Papaioannou, D. Kalpaxis, G.P. Dinos, C.M. Athanassopoulos, D.A. Missiri, P.C. Giannopoulou, I.A. Vlachogiannis, G.E. Papadopoulos, D. Papaioannou, D.L. Kalpaxis, Chloramphenicol derivatives as antibacterial and anticancer agents: historic problems and current solutions, Antibiotics 5 (2016) 20, https://doi.org/10.3390/antibiotics5020020.
[10] L.M. Guzman, D. Belin, M.J. Carson, J. Beckwith, Tight regulation, modulation, and high-level expression by vectors containing the arabinose pBAD promoter, J. Bacteriol. 177 (1995) 4121–4130 (Accessed November 14, 2018), http://www.ncbi.nlm.nih.gov/pubmed/7608087.
[11] D. Bulkley, C.A. Innis, G. Blaha, T.A. Steitz, Revisiting the structures of several antibiotics bound to the bacterial ribosome, Proc. Natl. Acad. Sci. U. S. A. 107 (2010) 17158–17163, https://doi.org/10.1073/pnas.1008685107.
[12] J.A. Dunkle, L. Xiong, A.S. Mankin, J.H.D. Cate, Structures of the Escherichia coli ribosome with antibiotics bound near the peptidyl transferase center explain spectra of drug action, Proc. Natl. Acad. Sci. U. S. A. 107 (2010) 17152–17157, https://doi.org/10.1073/pnas.1007988107.
[13] M.J. Weber, J.A. DeMoss, The inhibition by chloramphenicol of nascent protein formation in E. coli, Proc. Natl. Acad. Sci. U. S. A. 55 (1966) 1224–1230, https://doi.org/10.1073/PNAS.55.5.1224.
[14] E. Oh, A.H. Becker, A. Sandikci, D. Huber, R. Chaba, F. Gloge, R.J. Nichols, A. Typas, C.A. Gross, G. Kramer, J.S. Weissman, B. Bukau, Selective ribosome profiling reveals the cotranslational chaperone action of trigger factor in vivo, Cell 147 (2011) 1295–1308, https://doi.org/10.1016/j.cell.2011.10.044.
[15] Z. Kucan, F. Lipmann, Differences in Chloramphenicol sensitivity of cell-free amino acid polymerization systems, J. Biol. Chem. 239 (1964) 516–520 (Accessed November 14, 2018), http://www.ncbi.nlm.nih.gov/pubmed/14169152.
[16] Z. Alexieva, E.J. Duvall, N.P. Ambulos, U.J. Kim, P.S. Lovett, P.S. Lovett, Chloramphenicol induction of cat-86 requires ribosome stalling at a specific site in the leader, Proc. Natl. Acad. Sci. U. S. A. 85 (1988) 3057–3061.
[17] P.S. Lovett, Translation attenuation regulation of chloramphenicol resistance in bacteria — a review, Gene 179 (1996) 157–162, https://doi.org/10.1016/S0378-1119(96)00420-9.
[18] J. Marks, K. Kannan, E.J. Roncase, D. Klepacki, A. Kefi, C. Orelle, N. Vázquez-Laslop, A.S. Mankin, Context-specific inhibition of translation by ribosomal antibiotics targeting the peptidyl transferase center, Proc. Natl. Acad. Sci. U. S. A. 113 (2016) 12150–12155, https://doi.org/10.1073/pnas.1613055113.
[19] G.I. Makarov, T.M. Makarova, A noncanonical binding site of chloramphenicol revealed via molecular dynamics simulations, Biochim. Biophys. Acta - Gen. Subj. 2018 (1862) 2940–2947, https://doi.org/10.1016/J.BBAGEN.2018.09.012.
[20] M. Holm, A. Borg, M. Ehrenberg, S. Sanyal, Molecular mechanism of viomycin inhibition of peptide elongation in bacteria, Proc. Natl. Acad. Sci. U. S. A. 113 (2016) 978–983, https://doi.org/10.1073/pnas.1517541113.
[21] D.G. Dalbow, R. Young, Synthesis time of beta-galactosidase in Escherichia coli B/r as a function of growth rate, Bichem. J. (1975).
[22] X. Dai, M. Zhu, M. Warren, R. Balakrishnan, V. Patsalo, H. Okano, J.R. Williamson, K. Fredrick, Y.-P. Wang, T. Hwa, Reduction of translating ribosomes enables Escherichia coli to maintain elongation rates during slow growth, Nat. Microbiol. 2 (2017) 16231, https://doi.org/10.1038/nmicrobiol.2016.231.
[23] I.L. Volkov, M. Johansson, Single-molecule tracking approaches to protein synthesis kinetics in living cells, Biochemistry (2018), https://doi.org/10.1021/acs.biochem.8b00917.
[24] I.L. Volkov, M. Linden, J. Aguirre Rivera, K.W. Ieong, M. Metelev, J. Elf, M. Johansson, tRNA tracking for direct measurements of protein synthesis kinetics in live cells, Nat Chem Biol. (2018), https://doi.org/10.1038/s41589-018-0063-y.
[25] S.C. Blanchard, H.D. Kim, R.L. Gonzalez Jr., J.D. Puglisi, S. Chu, tRNA dynamics on the ribosome during translation, Proc. Natl. Acad. Sci. U. S. A. 101 (2004) 12893–12898, https://doi.org/10.1073/pnas.0403884101.
[26] D. Hanahan, J. Jessee, F.R. Bloom, Plasmid transformation of Escherichia coli and other bacteria, MethodsEnzym. 204 (1991) 63–113.
[27] P. Ranefall, S.K. Sadanandan, C. Wählby, Fast adaptive local thresholding based on ellipse fit, 2016 IEEE 13th Int. Symp. Biomed. Imaging, 2016, pp. 205–208, , https://doi.org/10.1109/ISBI.2016.7493245.
[28] G. Loy, A. Zelinsky, Fast radial symmetry for detecting points of interest, IEEE Trans. Pattern Anal. Mach. Intell. 25 (2003) 959–973, https://doi.org/10.1109/Tpami.2003.1217601.
[29] FASTRADIAL - Loy and Zelinski's fast radial feature detector, (n.d.). http://www.peterkovesi.com/matlabfns/Spatial/fastradial.m.
[30] M. Linden, V. Curic, E. Amselem, J. Elf, Pointwise error estimates in localization microscopy, Nat. Commun. 8 (2017) 15115, https://doi.org/10.1038/ncomms15115.
[31] K. Jaqaman, D. Loerke, M. Mettlen, H. Kuwata, S. Grinstein, S.L. Schmid, G. Danuser, Robust single-particle tracking in live-cell time-lapse sequences, Nat. Methods. 5 (2008) 695–702, https://doi.org/10.1038/nmeth.1237.
[32] K.P. Burnham, D.R. Anderson, Model Selection and Multimodel Inference: A Practical Information-theoretic Approach, second ed., Springer, New York, 2002.
[33] S.T. Liang, Y.C. Xu, P. Dennis, H. Bremer, mRNA composition and control of bacterial gene expression, J. Bacteriol. 182 (2000) 3037–3044 http://www.ncbi.nlm.nih.gov/entrez/query.fcgi?cmd=Retrieve&db=PubMed&dopt=Citation&list_uids=10809680.
[34] A. Borg, M. Ehrenberg, Determinants of the rate of mRNA translocation in bacterial protein synthesis, J. Mol. Biol. 427 (2015) 1835–1847 http://www.ncbi.nlm.nih.gov/pubmed/25451025.
[35] J. Chen, A. Petrov, A. Tsai, S.E. O'Leary, J.D. Puglisi, Coordinated conformational and compositional dynamics drive ribosome translocation, Nat. Struct. Mol. Biol. 20 (2013) 718–727, https://doi.org/10.1038/nsmb.2567.
[36] M. Johansson, E. Bouakaz, M. Lovmar, M. Ehrenberg, The kinetics of ribosomal peptidyl transfer revisited, Mol. Cell. 30 (2008) 589–598.
[37] H. Dong, L. Nilsson, C.G. Kurland, Co-variation of tRNA abundance and codon usage in Escherichia coli at different growth rates, J. Mol. Biol. 260 (1996) 649–663 http://www.ncbi.nlm.nih.gov/entrez/query.fcgi?cmd=Retrieve&db=PubMed&dopt=Citation&list_uids=8709146.
[38] M.C. Sulavik, C. Houseweart, C. Cramer, N. Jiwani, N. Murgolo, J. Greene, B. DiDomenico, K.J. Shaw, G.H. Miller, R. Hare, G. Shimer, Antibiotic susceptibility profiles of Escherichia coli strains lacking multidrug efflux pump genes, Antimicrob. Agents Chemother. 45 (2001) 1126–1136, https://doi.org/10.1128/AAC.45.4.1126-1136.2001.
[39] J.M. Andrews, Determination of minimum inhibitory concentrations, J. Antimicrob. Chemother. 48 (2001) 5–16, https://doi.org/10.1093/jac/48.suppl_1.5.
[40] I. Stock, B. Wiedemann, Natural antibiotic susceptibility of Escherichia coli, Shigella, E. vulneris, and E. hermannii strains, Diagn. Microbiol. Infect. Dis. 33 (1999) 187–199, https://doi.org/10.1016/S0732-8893(98)00146-1.
[41] S. Bakshi, A. Siryaporn, M. Goulian, J.C. Weisshaar, Superresolution imaging of ribosomes and RNA polymerase in live Escherichia coli cells, Mol. Microbiol. 85 (2012) 21–38, https://doi.org/10.1111/j.1365-2958.2012.08081.x.
[42] F. Balzarotti, Y. Eilers, K.C. Gwosch, A.H. Gynna, V. Westphal, F.D. Stefani, J. Elf, S.W. Hell, Nanometer resolution imaging and tracking of fluorescent molecules with minimal photon fluxes, Science (80-.) 355 (2017) 606–612, https://doi.org/

10.1126/science.aak9913.
[43] A. Sanamrad, F. Persson, E.G. Lundius, D. Fange, A.H. Gynna, J. Elf, Single-particle tracking reveals that free ribosomal subunits are not excluded from the Escherichia coli nucleoid, Proc. Natl. Acad. Sci. U. S. A. 111 (2014) 11413–11418, https://doi.org/10.1073/pnas.1411558111.
[44] R.J. Harvey, A.L. Koch, How partially inhibitory concentrations of chloramphenicol affect the growth of Escherichia coli, Antimicrob. Agents Chemother. (1980), https://doi.org/10.1128/AAC.18.2.323.
[45] J. Forchhammer, L. Lindahl, Growth rate of polypeptide chains as a function of the cell growth rate in a mutant of Escherichia coli 15, J. Mol. Biol. (1971), https://doi.org/10.1016/0022-2836(71)90337-8.
[46] K.B. Gromadski, M.V. Rodnina, Kinetic determinants of high-fidelity tRNA discrimination on the ribosome, Mol. Cell. 13 (2004) 191–200.
[47] V. Heurgué-Hamard, V. Dinçbas, R.H. Buckingham, M. Ehrenberg, Origins of minigene-dependent growth inhibition in bacterial cells, EMBO J. 19 (2000) 2701–2709, https://doi.org/10.1093/emboj/19.11.2701.
[48] L.R. Cruz-Vera, M.A. Magos-Castro, E. Zamora-Romo, G. Guarneros, Ribosome stalling and peptidyl-tRNA drop-off during translational delay at AGA codons, Nucleic Acids Res. 32 (2004) 4462–4468, https://doi.org/10.1093/nar/gkh784.